AD NUMBER

ADB008524

LIMITATION CHANGES

TO:

Approved for public release; distribution is unlimited.

FROM:

Distribution authorized to U.S. Gov't. agencies only; Test and Evaluation; 31 AUG 1975. Other requests shall be referred to Defense Advanced Research Projects Agency, Attn: TIO, Arlington, VA 22203.

AUTHORITY

DARPA ltr, 2 Apr 1982

Annúal Technical Report
for the Period 6/1/74 - 8/31/75

(12) (2) (12) 49 p.

(6) Acoustic Surface Wave Devices for Visible and Infrared Imaging,

(15) Grant Number DAHC15-73-G12,
Program Code No. 4D10 ARPA Order - 2340

Grantee: Purdue Research Foundation, Lafayette, In
(10) Principle Investigator: R. L. Gunshor (317) 493-9488

Effective Date of Grant: 6/1/74
Grant Expiration Date: 8/31/75 (11) 31 Aug 75
Amount of Grant: $99,910

(9) Annual technical rept. 1 Jun 74 - 31 Aug 75,

Sponsored by
Advanced Research Projects Agency
ARPA Order No. 2340 Amendment No. 1

Summary

The objective of this research is the conception, development and critical evaluation of a new class of devices employing the nonlinear interaction of acoustic surface waves (ASW) and photo-excited charge carriers to achieve rapid-scan optical imaging. The device operating principles are to be demonstrated initially through the use of silicon; however, a subsequent objective is to obtain imaging with infrared radiation using narrow bandgap semiconductors. The experimental effort involves both separate medium and monolithic device configurations.

The research is designed to emphasize the demonstration of newly envisioned device concepts for ASW imaging using silicon. The devices initially are fabricated using silicon in order to benefit from the well developed understanding and controllability of silicon surface properties. One of these devices, a transverse parametric imaging device, in addition to increased dynamic range, is expected to read an image in a time that is at least one-tenth of other proposed ASW devices.

A second device, for which operation is based on second harmonic generation, has been successfully operated as an imager, with significantly better performance than previously reported devices depending on attenuation to form the image. The actual advantage achieved by the second harmonic generation device was about 10 db, although as much as a 30 db increase in dynamic range is possible.

A study of a ZnO-silicon monolithic configuration for acoustic surface wave imaging was carried out in collaboration with the Naval Research Laboratory. The result of this effort is a convolver-type optical imaging device not requiring an air gap, and exhibiting a quite uniform interaction along the entire interaction length.

On the analytical side, a new large-signal convolution theory has been developed which will account for previously unexplained results from ASW convolution experiments.

Previously reported experimental results have been compared to theory for majority carrier mobility to demonstrate that acoustic surface waves can be used to explore charge particle motion in the surface region of a semiconductor.

The research program will continue to explore the above mentioned device concepts, and additionally provide critical evaluations of these and other ASW devices proposed for optical imaging, as compared to competing solid state imaging schemes.

Contents

I. Second Harmonic Generation for Optical Imaging*

(R. L. Gunshor, P. S. Schenker, C. W. Lee)

Recently reported ASW optical image devices transform spatial variations in light intensity to a corresponding set of amplitude variations in time on an electrical signal. This is accomplished by coupling rf surface waves propagating on a piezoelectric substrate to an adjacent semiconductor medium; the light-perturbed surface charge density is spatially variant along the path of ASW propagation. Reported devices differ in the wave-particle interaction phenomenon employed to obtain the image. This report concerns ASW conversion of optical images with light enhancement of second harmonic generation as the wave-particle interaction mechanism. Similar in configuration to the device reported by Moll, et al.,[1] the device described here employs two contrapropagating surface waves to form the converted image signal. One pulse serves as the power source for harmonic generation while another higher power pulse imparts image information to the harmonic by local decoupling of the semiconductor-ASW interaction. The second harmonic and its copropagating fundamental source will subsequently be referred to as reading signals; the higher power contrapropagating signal is termed a decoupling pulse.

The use of harmonic generation for optical imaging makes available the 40 db dynamic range associated with second harmonic generation of ASW in the presence of a semiconductor.[2] This effect portends a large harmonic signal amplitude variation for surface carrier density variations introduced by a given range of light intensity. In addition, unlike a device which is based on light-induced attenuation of the fundamental, output in the dark can approach zero.

*(This work is reported in Applied Physics Letters, Vol. 25, 688, December 15, 1974.)

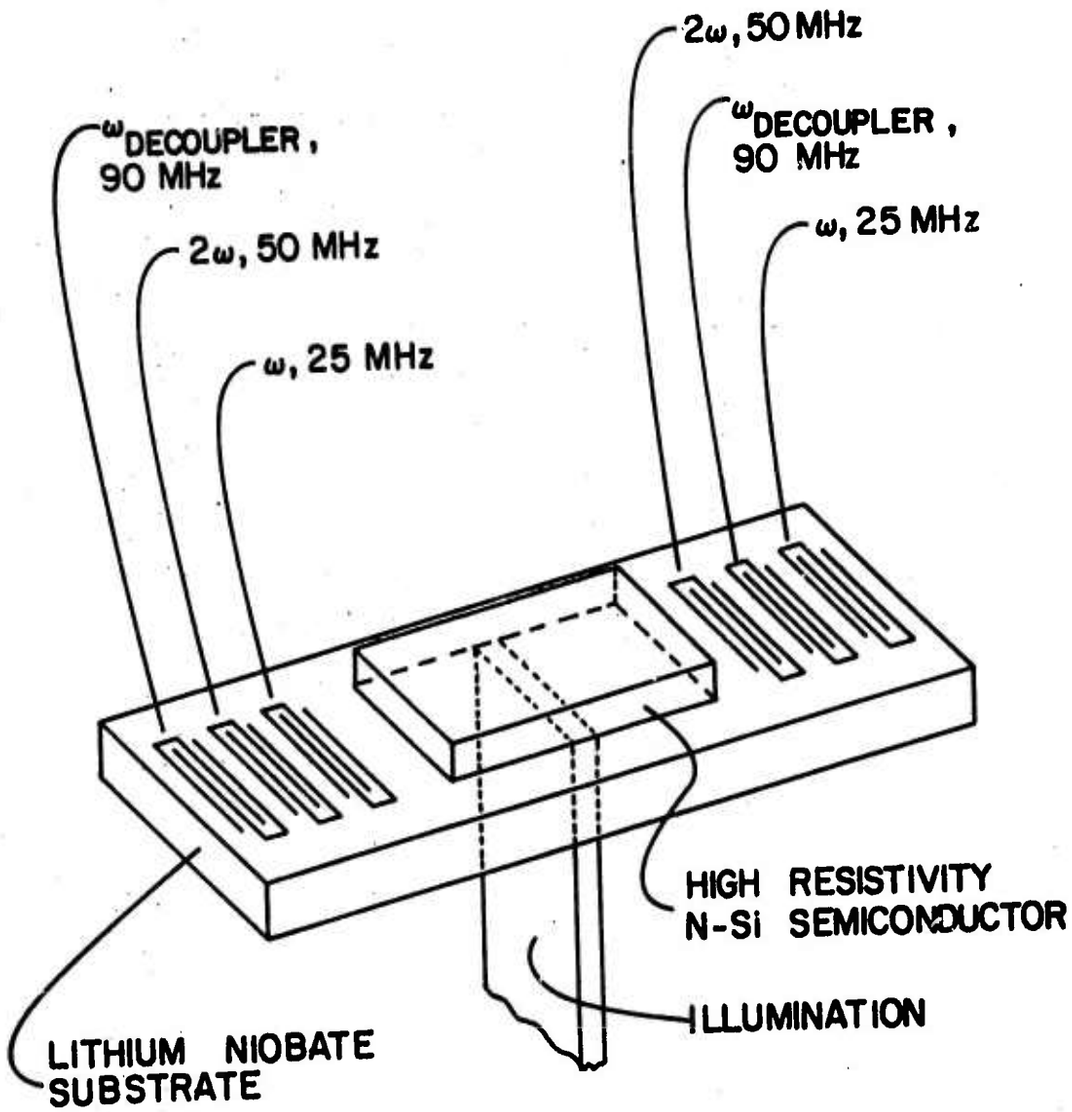

THE EXPERIMENTAL DEVICE

FIG.1-1 Experimental Device: Fundamental and Second Harmonic Frequencies are 25 and 50 MHz Respectively and Decoupler Input is at 90 MHz

Figure I-2 shows the image of two illuminated strips respectively 0.3 mm and 0.6 mm wide separated by 1.0 mm. The display is obtained using the second harmonic output scheme. The dimensions of strip widths and spacing correspond to two, four, and seven wavelengths at the fundamental frequency.

The level of illumination producing unity signal-to noise ratio in the second harmonic output is found to be about 6 db deblow 1 mW/cm^2 at 6328 Å.

A more complete description of the experiment was given in the Semi-Annual Technical Report.

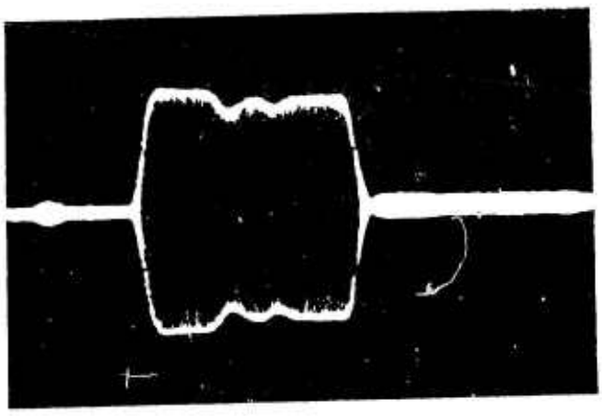

FIG. I-2 Second harmonic image of two slits.

References

1. N. J. Moll, O. W. Otto, and C. F. Quate, Journal de Physique, 33, Supplement to No. 11-12, 231 (1972).

2. C. W. Lee and R. L. Gunshor, Appl. Phys. Letts., 20, 288 (1972).

II. Optical Image Scanning with a ZnO-Si Monolithic Device+

(R. L. Gunshor, R. F. Pierret, J. K. Elliott, K. L. Davis*)

An optical image memory device using a zinc oxide-on-silicon surface acoustic wave convolver has recently been demonstrated.[1] The behavior of this structure was found to be strongly affected by the presence of a large number of traps associated with the zinc oxide. Measurements are presented in this report which indicate the presence of two distinct types of traps. In addition, an initialization procedure has been developed which permits the choice of the device operating point. It is shown that the device can either be used to image and store a fixed pattern, or it can be used to scan a nonstationary optical pattern without storage taking place.

Image scanning was achieved by using the surface wave convolver technique,[1-4] although alternative schemes for scanning optical images by means of propagating acoustic surface waves[5-7] have been used. Figure II-1 illustrates the configuration used for these experiments. The (111) cut silicon substrate is n-type with a bulk resistivity of 350 ohm-cm. Acoustic surface wave propagation is along $[2\bar{1}\bar{1}]$. The 0.1 micron SiO_2 layer was phosphorous gettered and then annealed under an aluminum film which was subsequently removed; the ZnO layer was rf diode sputtered to a thickness of approximately 1.2 micron. Optical images were focused onto the thin, semi-transparent aluminum convolver electrode. The maximum convolution efficiency obtained with this device (under optimum dc bias conditions) was -74 dBm. The 179 MHz two port delay line insertion loss (untuned) varied with bias from 26 dB in depletion to 30 dB in regions of accumulation and inversion where acoustoelectric absorption was strongest.

+To appear in Applied Physics Letters.
*Dr. Davis is with the Naval Research Laboratory, Washington D. C.

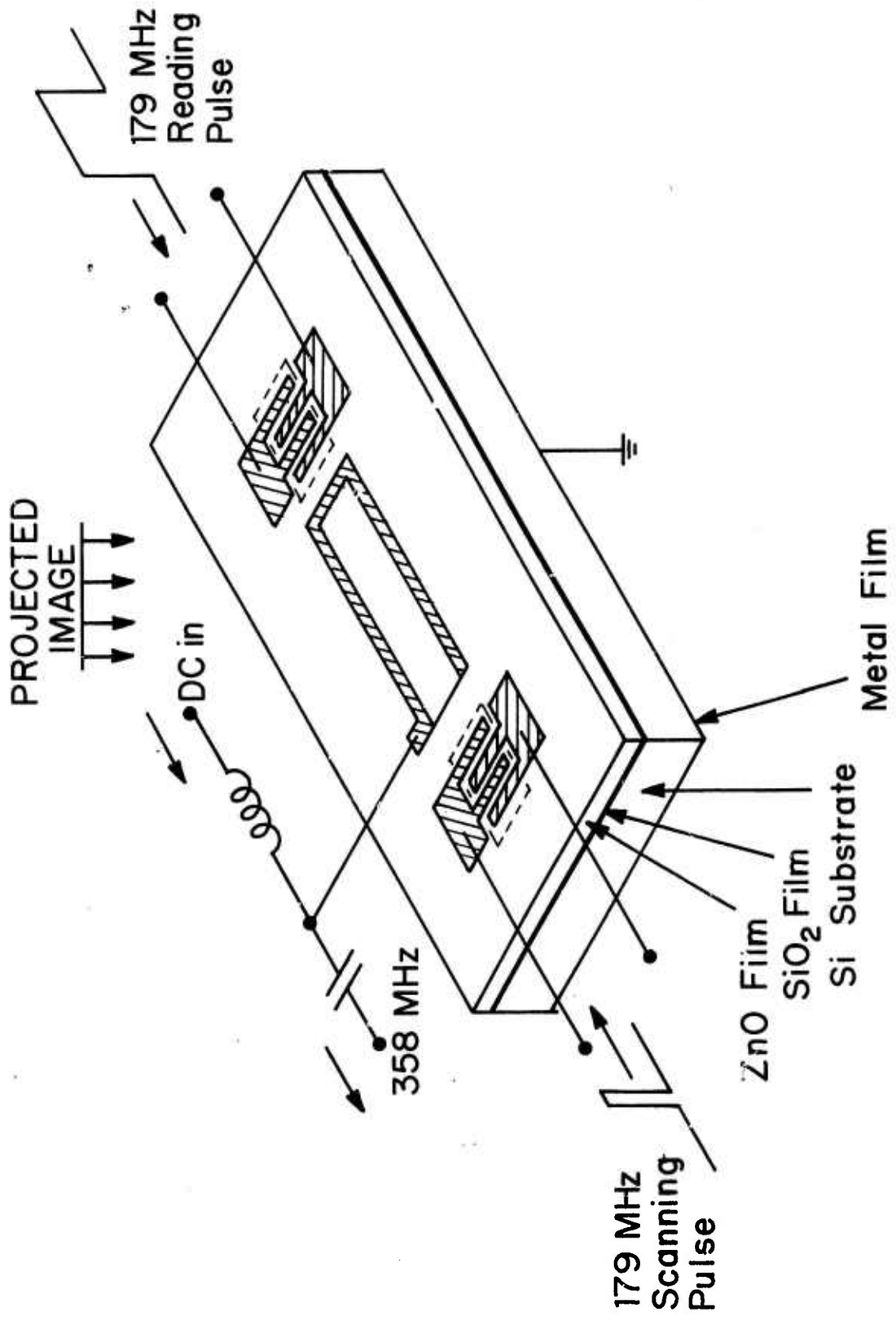
179 MHz
Reading
Pulse
PROJECTED
IMAGE
DC in
358 MHz
179 MHz
Scanning
Pulse
ZnO Film
SiO_2 Film
Si Substrate
Metal Film

Fig. II-1

A plot of convolver electrode capacitance vs. bias voltage is shown in Fig. II-2a. The characteristics of this curve are typical of the devices we have tested. The portions of the curve labeled A and B generally agree with results previously reported by Coldren.[8] As the bias voltage is varied from zero to more negative values, the capacitance follows curve A. With an applied negative bias, states in the ZnO and/or at the ZnO-SiO_2 interface charge via electron injection from the metal gate.[9] This charging is sufficient to shift the flat-band region of the curve to positive voltages. When the bias is changed in the positive direction, the capacitance follows curve B. Thus the magnitude of the trapped charge can be more than enough to compensate for the built-in positive charge. (This positive charge seems to be present in all of the devices, both n and p type, that we have fabricated to date.) These traps discharge very slowly; taking from one to three days for the flat band voltage to relax back to the equilibrium value (curve A). The magnitude of the voltage shift and the relaxation time are found to be strongly dependent on the size and duration of the negative bias voltage applied initially to the gate. A similar dependence was found by Coldren.[9] The relaxation is slightly accelerated by the application of a large positive gate bias, but it can be greatly accelerated by illuminating the device through the semi-transparent gate electrode. After generating curves A and B of Fig. II-2a, it is observed that white light illumination with zero bias voltage causes the flat-band capacitance to shift to the left. After 10 to 15 seconds of illumination the capacitance follows curve C when the voltage is again varied from zero to negative values. Additional illumination, even in combination with a positive bias, does not shift the flat-band point beyond curve C; at least a day in the dark is required for the device to relax completely back to curve A.

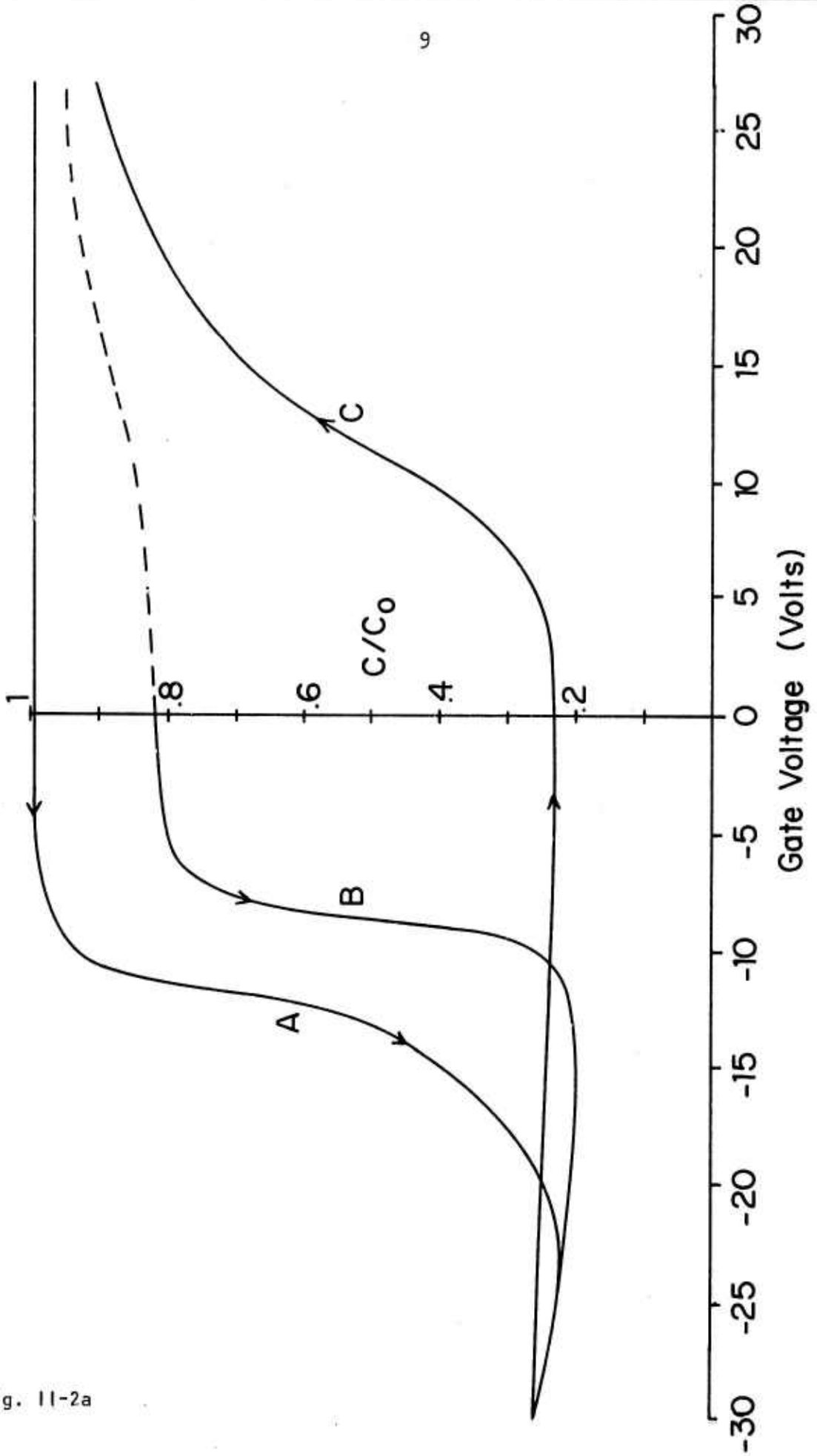
1
.8
.6
C/C₀
.4
.2
0
-5
-10
-15
-20
-25
-30
5
10
15
20
25
30
Gate Voltage (Volts)
A
B
C

Fig. II-2a

The data of Fig. II-2a can be used to identify two major types of states associated with the ZnO. Both types are charged by application of a negative bias to the gate electrode. One type of state discharges within about an hour in the dark or within about 15 seconds in white light, thus causing the capacitance characteristic to shift from curve B to C. The other type of state can remain charged for periods longer than a day. The discharge of the slower states is not noticeably accelerated by white illumination, but when initially uncharged, white light in combination with a small negative bias is found to charge these states.[1]

The above observations were used to establish a standardized procedure for initializing the device operating point so that stable and repeatable imaging could be performed. Initially the device was biased at -20 volts for five minutes; then the bias was reduced to zero and the convolver gate was illuminated with white light (100 mW/cm^2) for 15 sec. This procedure was used prior to obtaining the remainder of the data in this letter.

Figure II-2b illustrates the effect of light on the C-V characteristics of the imaging device after initialization.

The variation of second harmonic convolver output voltage as a function of dc bias level is shown in Fig. II-3a for relatively high-power input signals. This data was taken with 27 dBm, 1.5 μsec rf bursts applied to both input ports. The maximum convolver output appears to occur when the silicon surface is just changing from depletion to accumulation. There is a secondary maxima in the output at about -14 volts, which clearly occurs when the surface is inverted and where small signal convolver theory predicts zero output. It is in this region that optical minority carrier generation causes the greatest perturbation in the

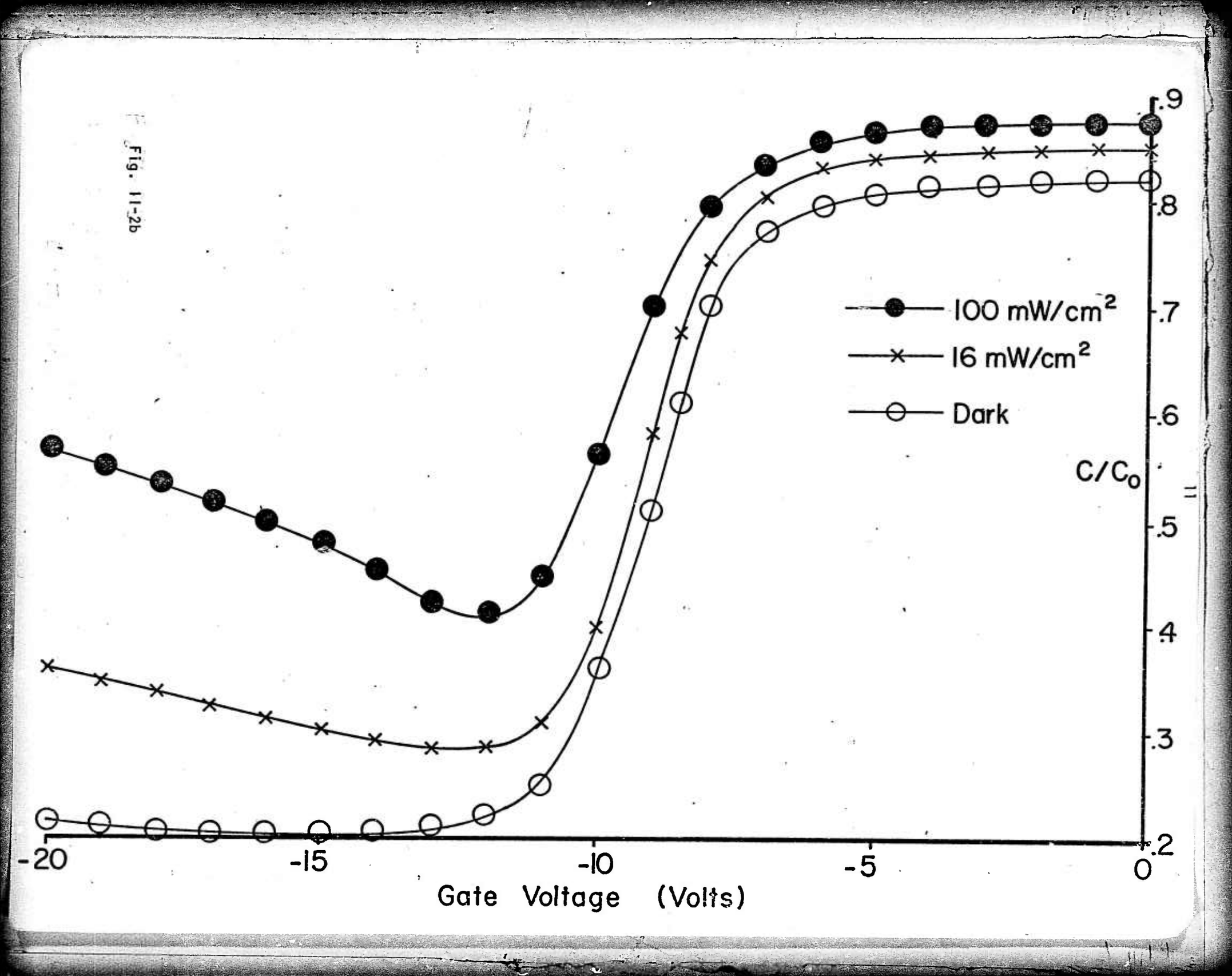
100 mW/cm²
16 mW/cm²
Dark
C/C₀
.9
.8
.7
.6
.5
.4
.3
.2
-20
-15
-10
-5
0
Gate Voltage (Volts)

Fig. II-2b

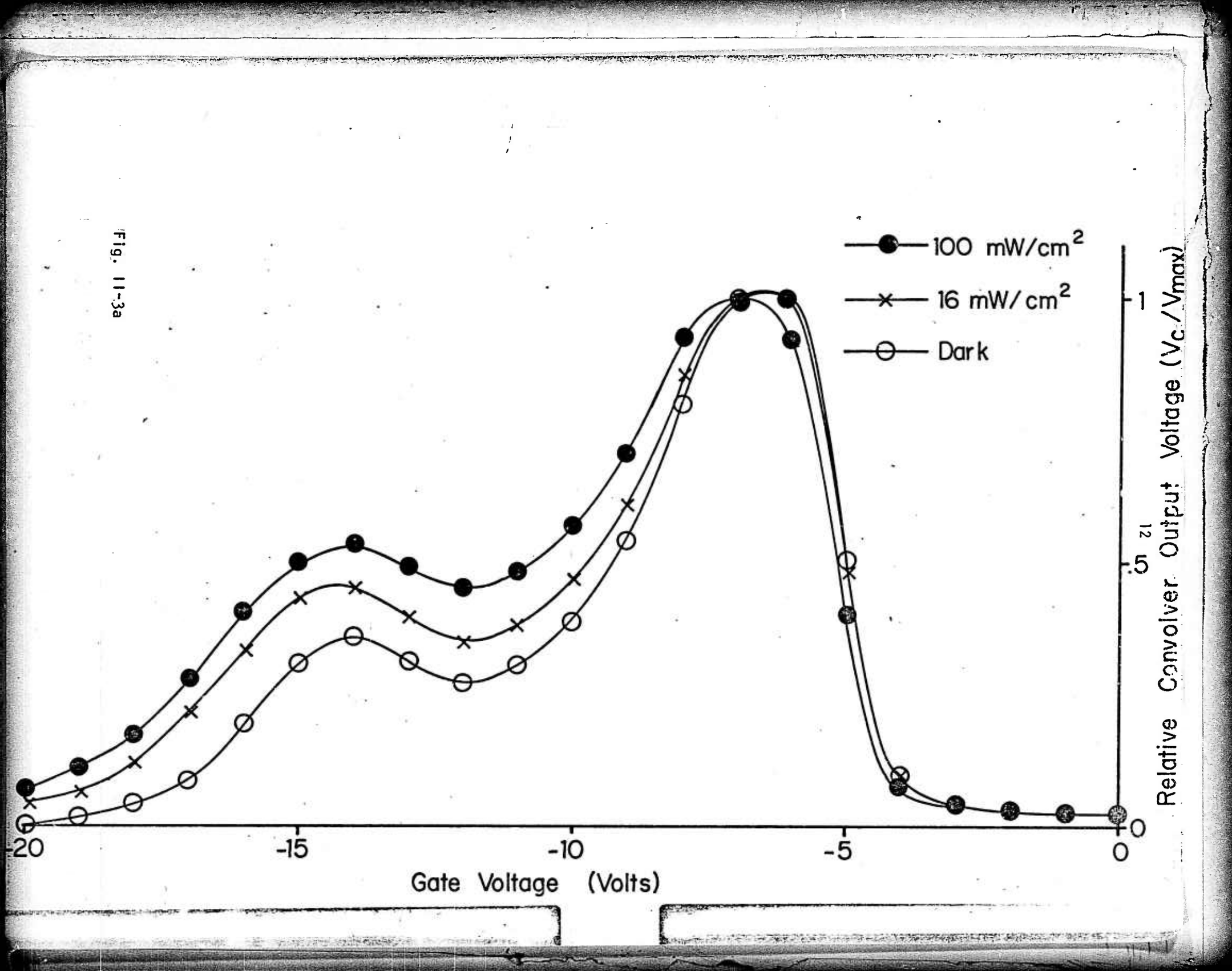
100 mW/cm²
16 mW/cm²
Dark
Relative Convolver Output Voltage (Vc/Vmax)
1
.5
0
-20
-15
-10
-5
0
Gate Voltage (Volts)

Fig. II-3a

Fig. II-3b

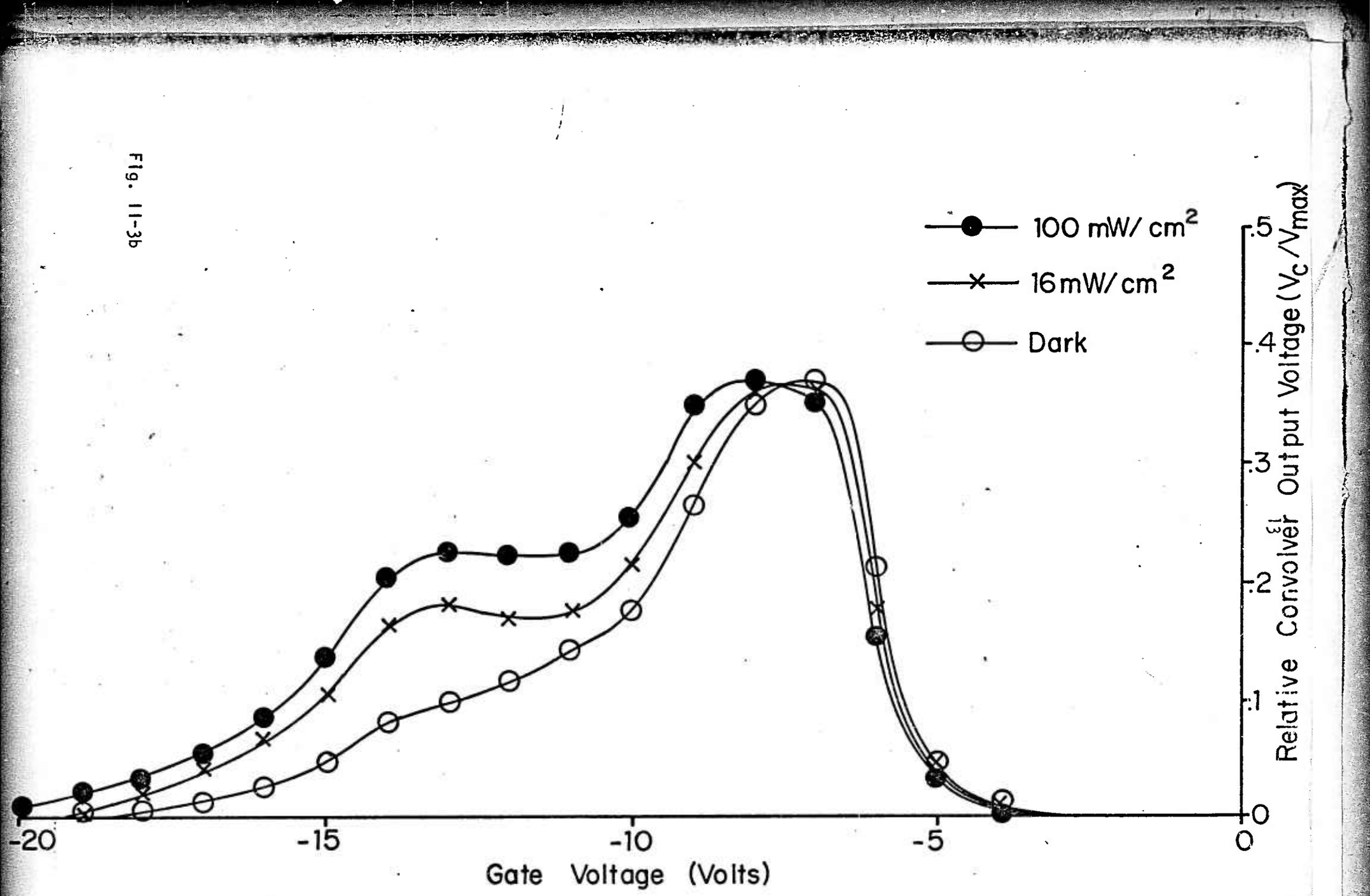
100 mW/ cm²
16 mW/ cm²
Dark
Relative Convolver Output Voltage (Vc/Vmax)
.5
.4
.3
.2
.1
0
-20
-15
-10
-5
0
Gate Voltage (Volts)

Fig. II-3c

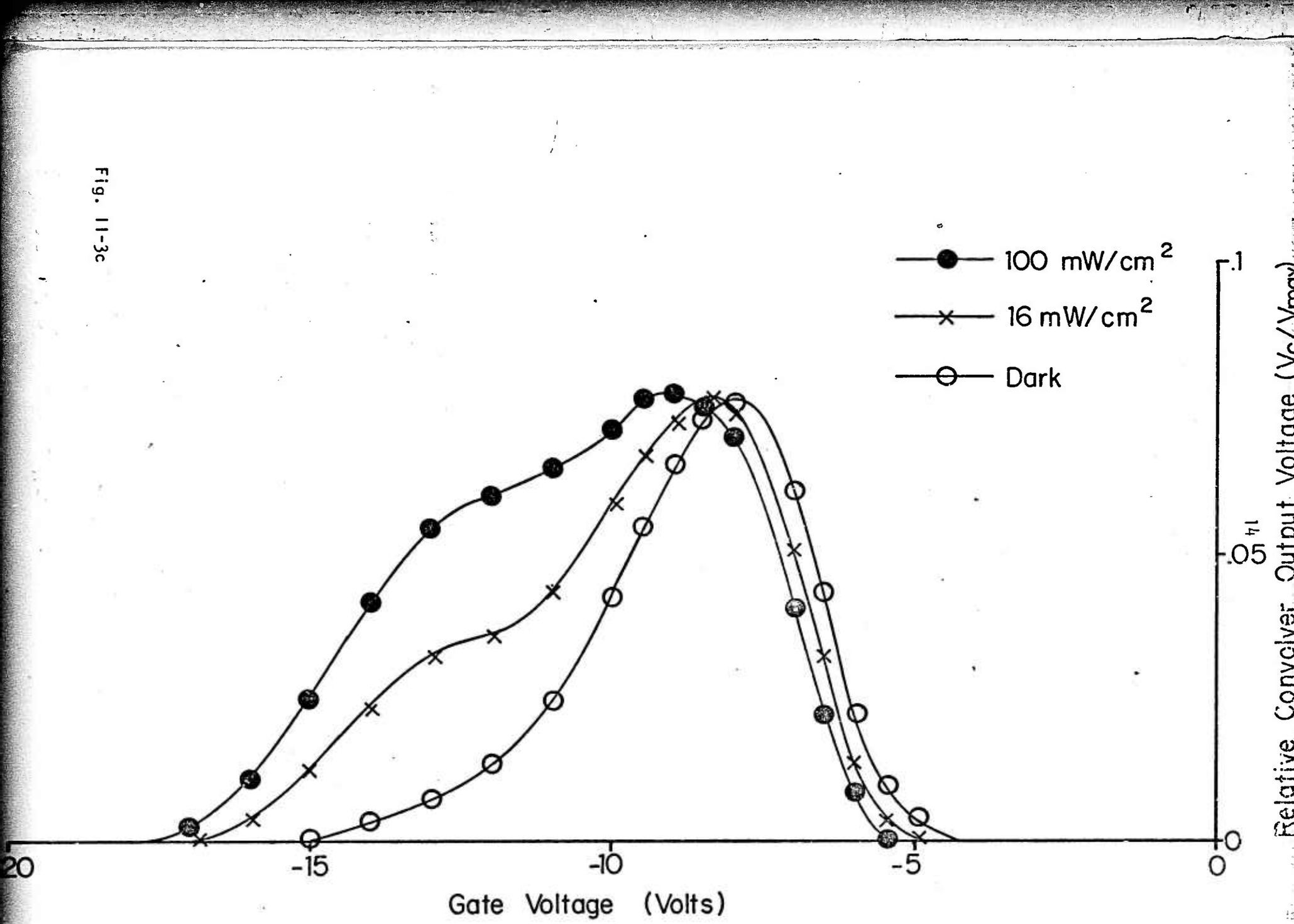
100 mW/cm 2
16 mW/cm 2
Dark
.1
.05
0
Relative Convolver Output Voltage (Vc/Vmax)
-20
-15
-10
-5
0
Gate Voltage (Volts)

convolver output. Similar data is presented in Fig. II-3b and II-3c for differing input power levels. Comparing the parts of Fig. II-3, it is noted that the relative magnitude of the light induced perturbations increases as input power is reduced. The shape of the characteristic in inversion also depends on the acoustic power level.

The sensitivity to light (both quantitative and qualitative) is found to be a strong function of dc bias level. For dc bias levels more negative than -7 volts, the perturbation in second harmonic output voltage varies with light intensity as shown in Fig. II-4. This dc bias region is designated the region of positive perturbation because the effect of illumination is to increase the convolver output voltage. Here the response to a varying illumination level is rapid, and a nonstationary image can be scanned. In contrast, when the bias level is between zero and -7 volts, the behavior is quite different. The perturbation in convolver output due to illumination is now negative and this region of negative perturbation displays a memory effect. When a strip of illumination is focused on the semiconductor with bias in the region of negative perturbation, a "dip" in the trapazoidal output is observed. This dip will increase with time until the output is zero in the illuminated region, taking about 10 seconds to reach zero at an illumination level of 100 mW/cm^2. The image, apparently the result of photon integration, is then stored in the system for periods longer than a day. The region of positive perturbation is the most desirable operating range for scanning a nonstationary image using this device since there is no memory in this region. The data for Fig. II-4 was taken with the same acoustic surface wave input power levels used for the image scanning shown in Fig. II-5: a reading pulse of 17.6 dBm and 2.4 μsec duration, and a scanning pulse

Fig. 11-4

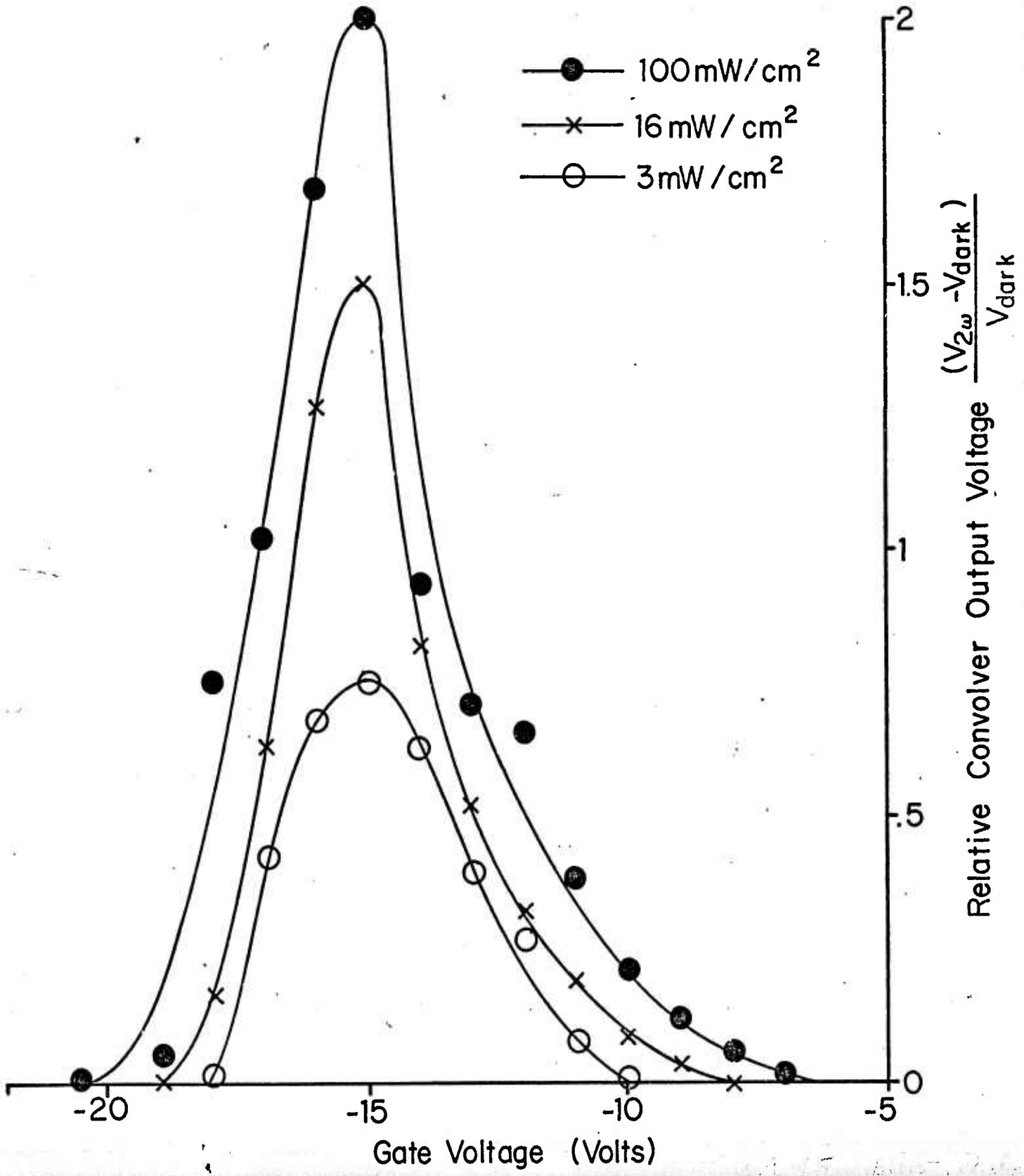
100 mW/cm²
16 mW/cm²
3 mW/cm²
2
1.5
1
.5
0
-20
-15
-10
-5
Gate Voltage (Volts)
Relative Convolver Output Voltage (V2ω - Vdark) / Vdark

of 27.6 dBm and 0.1 μsec duration. The behavior of the convolver output as a function of bias for these operating conditions was similar to the data of Fig. II-3.

Figure II-5 shows a one dimensional image (line scan)[10] detected by the device characterized in the previous figures. Note that the convolution output is limited in duration by the length of the reading pulse used. A longer reading pulse would allow imaging over the entire length of the integrating gate; the pulse duration used here was reduced to avoid overlapping a spurious signal. The scanned image consists of three strips of white illumination (100 mW/cm^2) separated by 1.0 mm and having widths of 0.2 mm, 0.6 mm, and 0.2 mm, respectively. This projected image was mechanically swept across the device to demonstrate image scanning. The dc bias used was -11.5 volts. The overall sensitivity to light increases to a maximum at -14 volts; however at bias voltages this far into inversion, some degradation in spatial resolution results from lateral charge transport. The bias value of -11.5 was chosen to optimize sensitivity (unity signal-to-noise is obtained at an illumination of 3 mW/cm^2) and resolution.

We conclude that it is feasible to perform optical image scanning with acoustic surface waves using a monolithic silicon structure. Nonstationary patterns can be imaged, or if desired, a fixed pattern could be stored using this structure. For applications where memory is not required, device stability can probably be improved by depositing an insulating layer between the gate electrode and the ZnO film to block electron injection into the ZnO. Dynamic range could be improved by decreasing output in the dark using the techniques reported in reference 2. In addition, the sensitivity and resolution of this initial device prototype could be greatly enhanced by design improvements enabling effective use of a narrower scanning pulse.

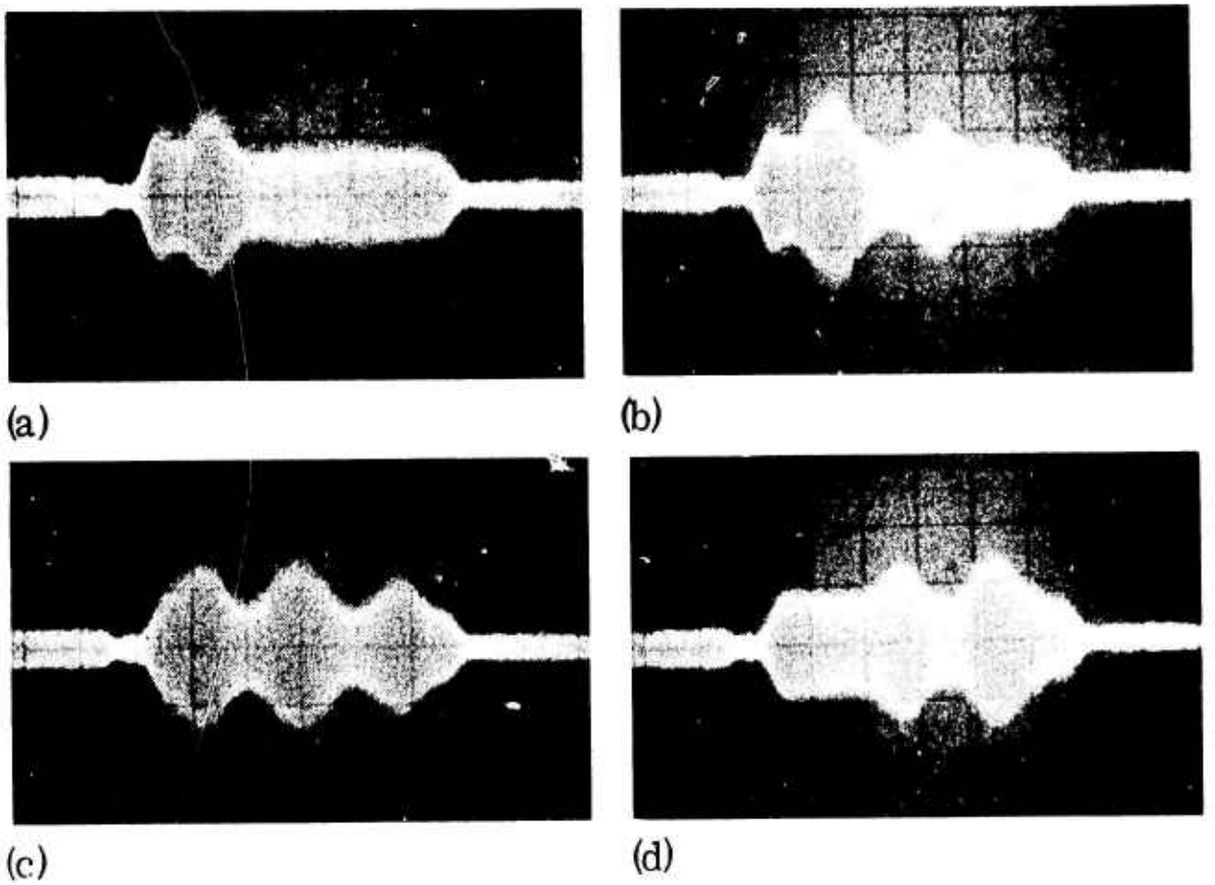

Fig. II-5

Figure Captions

Fig. II-1 Monolithic image scanner device configuration.

Fig. II-2 (a) Capacitance (at 1 MHz) of ZnO-SiO_2-Si structure versus gate bias voltage under the following conditions: A - measurement taken with device initially in equilibrium; B - measurement taken after 5 minute -20 V bias; C - measurement taken after 15 sec. white illumination with zero bias.
(b) Capacitance (at 1 MHz) of ZnO-SiO_2-Si structure versus gate bias voltage for difference light intensities.

Fig. II-3 Second harmonic output versus gate bias for the light intensities of Fig. 2b. Measurement made using identical input pulses of 1.5 μs each and the following power: (a) 27 dBm; (b) 19.5 dBm; (c) 9.6 dBm.

Fig. II-4 Second harmonic convolver output in excess of the output in the dark as a function of gate bias for three light intensities. The data has been normalized to the value in the dark.

Fig. II-5 Optical image scan of pattern described in text for 4 positions of the image. The horizontal scale is 0.2 μs/division.

References

1. K. L. Davis, Appl. Phys. Lett. 26, 143 (1975).

2. H. Gautier, G. S. Kino, and H. J. Shaw, Proc. 1974 IEEE Ultrasonics Symposium, p. 99.

3. T. W. Grudkowski and C. F. Quate, Appl. Phys. Lett. 25, 99 (1974).

4. N. J. Moll, O. W. Otto, and C. F. Quate, J. Phys. (Paris) Suppl. 33, No. 11-12, 231 (1972).

5. S. Takada, H. Haykawa, and N. Mikoshiba, Appl. Phys. Lett. 23, 415 (1973).

6. M. Luukkala and P. Merilainen, Electron. Lett. 10, 80 (1974).

7. P. S. Schenker, C. W. Lee, and R. L. Gunshor, Appl. Phys. Lett. 25, 688 (1974).

8. L. A. Coldren, Appl. Phys. Lett. 25, 473 (1974).

9. L. A. Coldren, Appl. Phys. Lett. 26, 137 (1975).

10. Two dimensional imaging may be achieved by mechanical scanning in the second dimension, or by means of an array of parallel convolver gates.

III. Large-Signal Acoustic Surface Wave (ASW) Convolver Response Theory

(R. F. Pierret and R. L. Gunshor)

1. INTRODUCTION

The acoustic surface wave (ASW) structure known as the convolver has received considerable attention recently because of its projected use in signal processing and imaging applications. In evaluating its potential in such applications, and in design considerations, a simple response theory for the convolver is clearly desirable. Various operational theories have been formulated, the most tractable of which is the small signal equivalent circuit formulation developed by Kino et. al. The small signal approach, however, suffers from the questionable general validity of the small signal approximation. Even though the output of the convolver at twice the fundamental input signal may indeed be small in size, the excursions of the semiconductor surface potential inside the structure at the fundamental frequency may often preclude the use of the small signal approximation. Furthermore, the separate computation of an open circuit signal source and the subsequent incorporation of the signal source into an empirically derived equivalent circuit leads to a somewhat complex model for arbitrary d.c. biasing of the convolver gate.

Herein we present a relatively simple large-signal ASW convolver response theory which emphasizes the similarity between the ASW convolver structure and metal-insulator-semiconductor (MIS) devices. MIS device modeling and formalism is first used to obtain a large signal circuit representation for the ASW convolver, and this in turn is used to derive the

control equation specifying the convolver's large signal response. Subsequently, the small signal limit is invoked to provide a basis for comparison with earlier theories. A direct correspondence between the convolver output and the small-signal convolver gate capacitance, a correspondence noted in the experimental work by Coldren, is also established and clearly exhibited. Finally, operation of the convolver when the convolver gate is inversion biased, a bias region which has been heretofore neglected or unproperly characterized, is discussed in terms of MIS-capacitor transient characteristics and charge-coupled-device (CCD) like action.

2. LARGE SIGNAL CIRCUIT DERIVATION

Following previous formulations, the dominant effect of the traveling surface waves pictured in Fig. 1, the dominant effect as far as the convolver structure is concerned, is taken to be the establishing of transverse electric fields at the semiconductor surface of the form

$$E_{x1}(y, t) = E_{w1} \cos (ky - \omega t) \tag{1a}$$

$$E_{x2}(y, t) = E_{w2} \cos (ky + \omega t) \tag{1b}$$

Assuming for simplicity $E_{w1} = E_{w2} = E_w$, the total surface electric field in the region where the waves overlap will be

$$E_x(y, t) = E_w \cos (ky - \omega t) + E_w \cos (ky + \omega t) \tag{2a}$$

$$= 2E_w \cos ky \cos \omega t \tag{2b}$$

In the overlap region there therefore exists a standing-wave electric field perturbation external to the semiconductor surface. This standing wave region is of course the active portion of the device giving rise to the convolver output.

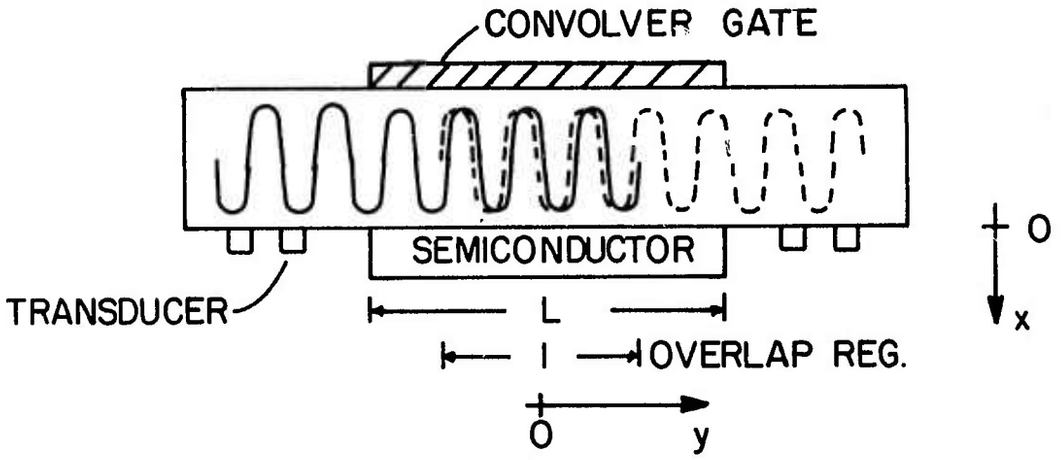

FIG. III-1

Simplified cross section of an ASW convolver picturing acoustic surface wave propagation. The figure also specifies the assumed coordinate system and pertinent geometrical features.

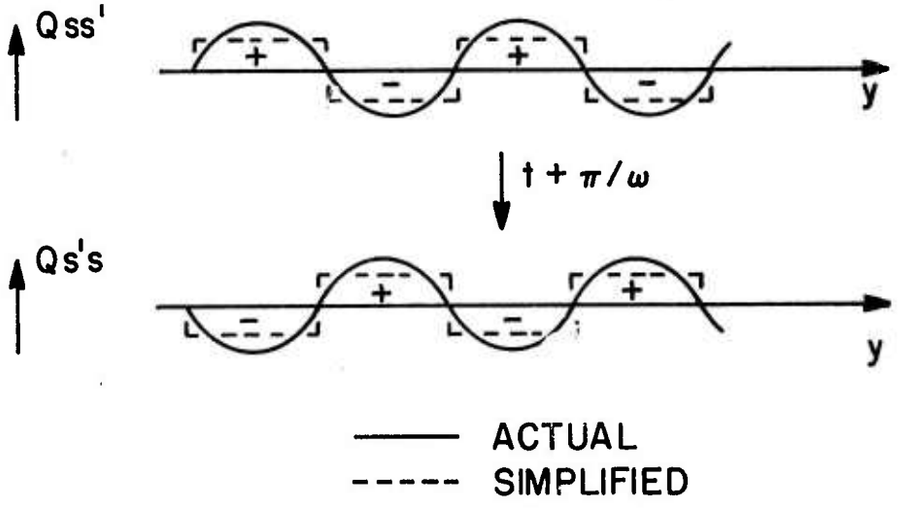

FIG. III-2

Variation of the effective ASW-induced "surface state" charge as a function of position and time.

We next note that the appearance of a standing-wave E_x-field pattern at the semiconductor's external surface is functionally equivalent (in a one-dimensional analysis of normal to the surface electrostatic variables inside the semiconductor) to placing a surface charge per cm^2, Q'_{ss}, of magnitude

$$Q'_{ss}(y, t) = K_I \epsilon_0 E_x (y, t) \tag{3a}$$

$$= 2K_I \epsilon_0 E_w \cos ky \cos \omega t \tag{3b}$$

over the surface of the semiconductor in the overlap region. K_I represents the dielectric constant of the insulator immediately adjacent to the semiconductor and ϵ_0 is the permittivity of free space. Hence, the net effect of the overlapping acoustic surface waves may be alternately characterized in terms of an effective surface state charge. The charge when averaged over a wavelength exhibits a net zero value and can be conceived to "slosh" back and forth as a function of time between half-wavelength regions (see Fig. 2).

At this point we will simplify the subsequent analysis by replacing the Q'_{ss} charge appearing in any given half-wavelength region by a uniform charge distribution equal to the average value of $Q'_{ss}(y, t)$ within the half-wavelength region; i.e.,

$$Q'_{ss} \rightarrow \pm \frac{4}{\pi} K_I \epsilon_0 E_w \cos \omega t \tag{4}$$

The indicated simplification (also pictured in Fig. 2) could be omitted in the theoretical development. However, a more exact analysis is questionable considering our initial use of a simplified representation for the E-field at the semiconductor's surface and the general one-dimensional nature of the entire analysis.

Now, and this a critical step in the derivation, to achieve the same degree of semiconductor band bending, it is readily shown that the voltage v_G actually applied to the gate of an MIS structure possessing surface states is rated to the voltage v_G' applied to an ideal device (no surface states) by

$$v_G = v_G' - \frac{Q_{ss}}{C_i} \tag{5}$$

where C_i is the insulator capacitor per unit area. This may alternately be interpreted as saying a MIS structure with surface states and biased to a voltage v_G can be conceptually replaced by a MIS structure without surface states biased to a gate potential of $v_G' = v_G + v_0$, where $v_0 = Q_{ss}/C_i$. Making the obvious extension to the ASW convolver, each half-wavelength region possessing a standing wave can be modeled as a MIS capacitor free of a semiconductor surface perturbation but subject to a gate driving potential

$$v_G = v_G \text{ (external circuit)} \pm V_0 \cos \omega t \tag{6}$$

$$V_0 = \frac{\frac{4}{\pi} K_1 \epsilon_0 E_w}{C_i} = \frac{4}{\pi} x_i E_w \tag{7}$$

where x_i is the insulator thickness.* Summing equivalent wavelength regions over the overlap length, l, one then deduces the basic convolver representation shown in Fig. 3a. As displayed in Fig. 3b, the entire large signal circuit representation is completed by adding external circuit components, a resistance R_B to model the semiconductor bulk resistance, and a

* ASW convolvers are commonly constructed with two insulating layers between the gate and semiconductor. If this be the case then x_i is to be interpreted as an effective insulator thickness equal to $x_{i1} + (K_{I1}/K_{I2})\, x_{i2}$, where subscript 1 refers to the insulator immediately adjacent to the semiconductor and subscript 2 refers to the insulator immediately adjacent to the gate.

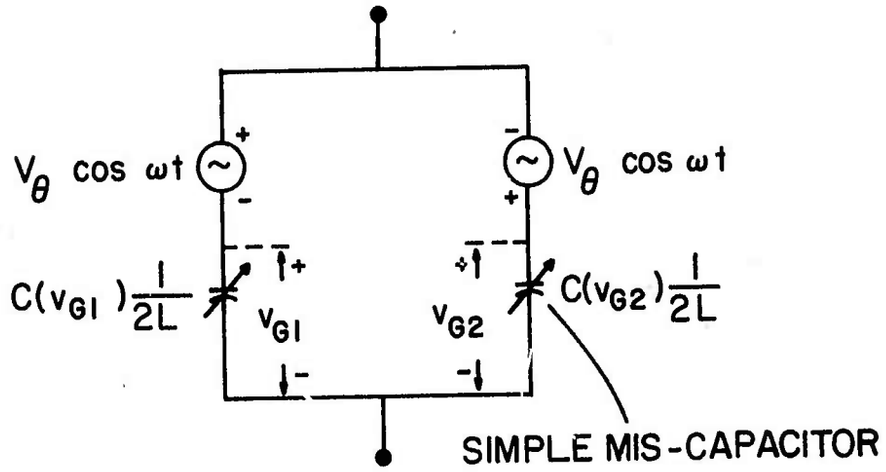

FIG. III - 3a

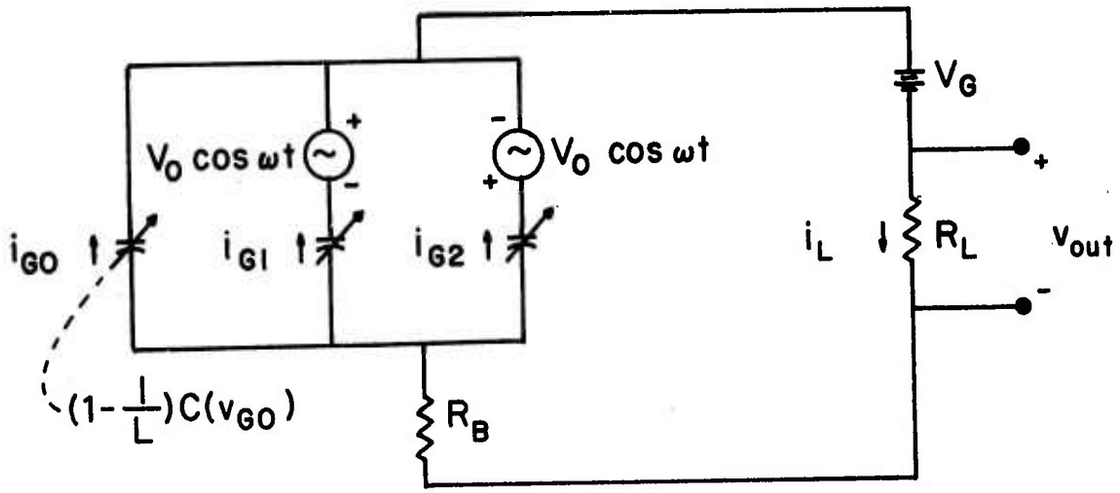

FIG. III - 3b

Large signal circuit representation for the ASW convolver. (a) Overlap region equivalent circuit; (b) total circuit.

shunting capacitance (1-1/L) C (v_{G0}) to account for the gate capacitance in the non-overlap region.

In examining Fig. 3b note that, in agreement with experimental observations, the inverted phase relationship of the V_0 cos ωt driving voltages and the identical nature of the varactors in the basic circuit automatically leads to a v_{out} at only even harmonics of the fundamental frequency ω. Furthermore, at d.c. biases where V_G heavily accumulation biases the structure and V_0 is of insufficient magnitude to offset this bias on the MIS-C's, $C(v_{G1}) = C(v_{G2}) = C_I$ (the insulator capacitance) = a constant at all times and $v_{out} \simeq 0$. If V_G is systematically varied from accumulation toward inversion, it is readily deduced, recalling in addition the well known C-V_G dependence of an MIS-C, that v_{out} will increase from zero, peak at the V_G gate bias corresponding to the maximum variation in the varactor capacitances for a given V_0, and then decrease again as V_G approaches the inversion bias point. Under inversion biasing there is an interaction between half-wavelength semiconductor regions in the convolver structure and the capacitance exhibited by the MIS varactors appearing in the Fig. 3a model must be given additional consideration. A discussion of the convolver response in the inversion bias range is therefore handled separately and is deferred to a later section.

3. LARGE SIGNAL RESPONSE

Referring to Fig. 3, circuit considerations yield

$$v_{out}(t) = i_L R_L \tag{8}$$

$$i_L = i_{G0} + i_{G1} + i_{G2} \tag{9}$$

and

$$v_{G0} = V_G + v_{out}(R_L + R_B)/R_L \tag{10a}$$

$$v_{G1} = V_G + v_{out}(R_L + R_B)/R_L - V_0 \cos \omega t \tag{10b}$$

$$v_{G3} = V_G + v_{out}(R_L + R_B)/R_L + V_o \cos \omega t \tag{10c}$$

Furthermore, considering the MIS varactors

$$i_{G0} = - \frac{dq_{G0}}{dt} = - \frac{dq_{G0}}{dv_{G0}} \frac{dv_{G1}}{dt} \tag{11}$$

q_G being the gate charge, or

$$i_{G0} = - (1 - \frac{1}{L}) C(v_{G0}) \frac{dv_{G0}}{dt} \tag{12a}$$

and

$$i_{G1} = - \frac{1}{2L} C(v_{G1}) \frac{dv_{G1}}{dt} \tag{12b}$$

$$i_{G2} = - \frac{1}{2L} C(v_{G2}) \frac{dv_{G2}}{dt} \tag{12c}$$

Combining eqs. (8)-(10) and (12) one obtains

$$(R_L + R_B) [(1 - \frac{1}{L}) C(v_{G0}) + \frac{1}{2L} C(v_{G2})] \frac{dv_{out}}{dt}$$

$$+ v_{out} + \frac{1}{2L} R_L [C(v_{G1}) - C(v_{G2})] V_0 \omega \sin \omega t = 0 \tag{13}$$

Eq. (13) [in conjunction with eqs. (10) and the MIS-C C-V_G relationship] is the large signal control equation which must be solved numerically to obtain the periodic variation of $v_{out}(t)$. Once this has been accomplished, $v_{out}(2\omega)$, the 2ω component of interest in theoretical-experimental comparisons, can be readily extracted by standard Fourier analysis techniques. Large signal computational results will not be presented herein but are planned for a subsequent publication containing experimental results.

4. THE SMALL SIGNAL UNIT

In the small signal limit the MIS-C capacitances can be expanded in a Taylor series about the d.c. dias point to obtain*

$$C(v_{G0}) \simeq C(V_G) + \frac{dc}{dV_G}\left[v_{out}\left(\frac{R_L + R_B}{R_L}\right)\right] \tag{14a}$$

$$C(v_{G1}) \simeq C(V_G) + \frac{dc}{dV_G}\left[v_{out}\left(\frac{R_L + R_B}{R_L}\right) - V_0 \cos \omega t\right] \tag{14b}$$

$$C(v_{G3}) \simeq C(V_G) + \frac{dc}{dV_G}\left[v_{out}\left(\frac{R_L + R_B}{R_L}\right) + V_0 \cos \omega t\right] \tag{14c}$$

giving in turn

$$\left(1 - \frac{1}{L}\right) C(v_{G0}) + \frac{1}{2L} C(v_{G1}) + \frac{1}{2L} C(v_{G2}) \simeq C(V_G) \tag{15}$$

and

$$C(v_{G1}) - C(v_{G2}) = -2\frac{dc}{dV_G} V_0 \cos \omega t \tag{16}$$

Hence, in the small signal limit eq. (13) simplifies to

$$\tau \frac{dv_{out}}{dt} + v_{out} = V_N \sin 2\omega t \tag{17}$$

$$\tau \equiv (R_L + R_B)\, C\,(V_G) \tag{18}$$

$$V_N \equiv \frac{1}{2L} R_L \frac{dc}{dV_G} V_0^2\, \omega \tag{19}$$

---

* Note that the $dC/dv_{Gj}/V_G$ (j = 1, 2, 3), which should actually appear in the Taylor series expansions, have been replaced by dC/dV_G. In an accumulation or depletion biased ideal MIS structure dC/dv_G is identically equal to dC/dV_G. For the same bias range in a real MIS structure operated at ASW convolver frequencies dC/dv_G will be equal to the voltage derivative of the structure's ideal C-V_G relationship. In other words, dC/dV_G in eqs. (14) must be interpreted as the voltage derivative of the ASW convolver's ideal C-V_G characteristic and not the voltage derivative of the observed C-V_G characteristic.

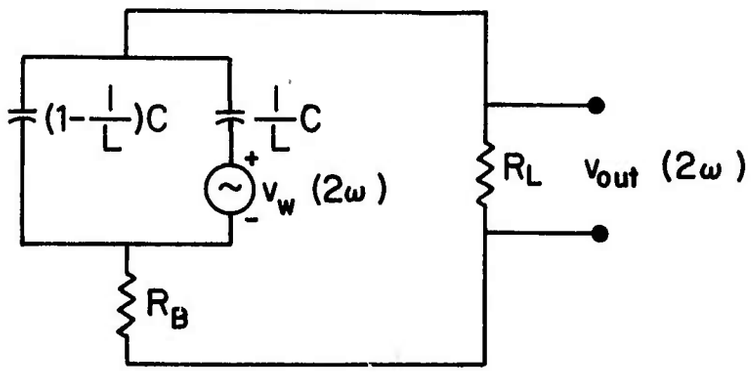

FIG. III-4

ASW convolver small signal equivalent circuit.

The periodic solution of eq. (17) is readily established to be

$$v_{out}(t) = \frac{V_N}{\sqrt{1 + (2\omega\tau)^2}} \sin(2\omega t + \phi) \tag{20}$$

where ϕ is a constant phase factor for a given set of operating conditions. The magnitude of the small signed 2ω output is thus predicted to be

$$v_{out}(2\omega) = \frac{|V_N|}{\sqrt{1+(2\omega\tau)^2}} \tag{21a}$$

$$= \left[\frac{1}{2L}\left(\frac{4x_i}{\pi}\right)^2 \omega R_L E_w^2 \left|\frac{dc}{dV_G}\right|\right] / \sqrt{1 + [2(R_L + R_B)C]^2} \tag{21b}$$

Upon examining the preceding result one notes that $v_{out}(2\omega)$ is proportional to the overlap length (l) and the product of the ASW field magnitudes (E_w^2) in agreement with other analyses. In addition, subject to the qualification presented in a footnote earlier in this section, the output should be directly proportional to the slope of the small signal C-V_G characteristics derived from the convolver gate. This is precisely the general behavior observed by Coldren. Finally, previous analyses have modeled the 2ω small signal response in terms of the small signal equivalent circuit shown in Fig. 4. Clearly, the output predicted by the Fig. 4 model and that obtained herein are identical if one sets

$$v_w(2\omega) = \frac{V_0^2}{4C}\left|\frac{dc}{dV_G}\right| \tag{22}$$

where $v_w(2\omega)$ is the magnitude of the small signal voltage generation appearing in the Fig. 4 model.

5. COMPUTATIONAL RESULTS

Sample computational results of $v_{out}(2\omega)/V_0^2$ vs. V_G at selected signal levels (as specified by V_0) are displayed in Fig. 5(a). The corresponding theoretical high-frequency C-V_G characteristic is also shown in Fig. 5(b) for reference purposes. The system parameters used in the computations, it should be noted, are those of a monolithic ZnO-SiO_2-Si convolver presently under investigation in our laboratories. (A complete list of assumed structural and measurement parameters has been tabulated in Appendix 1.) The three circled points appearing in Fig. 5(a) represent exact large signal results obtained from a direct numerical solution of eq. (13); the remainder of the plot, including the small signal limit, was constructed employing an approximate solution which will be detailed below. As a computational check, the small signal output was also calculated directly from eq. (21), using a separate computer routine, and was found to be identical to the corresponding approximate solution output plotted in Fig. 5(a).

The approximate solution to which we have been referring is based on two simplifications. (1) The convolver output $[v_{out}(t)]$ is assumed negligible compared to the d.c. and $V_0\cos\omega t$ voltages appearing in eq. (10), permitting one to write

$$v_{G0} \simeq V_G \tag{23a}$$

$$v_{G1} \simeq V_G - V_0\cos\omega t \equiv v_{G-} \tag{23b}$$

$$v_{G2} \simeq V_G + V_0\cos\omega t \equiv v_{G+} \tag{23c}$$

(2) The time varying coefficient of dv_{out}/dt in eq. (13) is approximated by a time constant, $\bar{\tau}$, obtained by time averaging the dv_{out}/dt coefficient over the period of a cycle.

Utilizing the cited simplifications eq. (13) reduces to

$$\bar{\tau}\frac{dv_{out}}{dt} + v_{out} = \frac{\ell}{2L} R_L \left[C(v_{G+}) - C(v_{G-})\right] V_0 \omega \sin\omega t \tag{24}$$

This simplified control equation can readily be solved, and the solution subsequently manipulated, to obtain

$$v_{out}(2\omega) = \frac{|V_N|}{\left[1 + (2\omega\bar{\tau})^2\right]^{1/2}} \tag{25}$$

where

$$\bar{\tau} \equiv (R_L+R_B)\left\{G(V_G) + \frac{\ell}{2L}\frac{1}{\pi}\int_0^{\pi}\left[C(v_{G+}) + C(v_{G-}) - 2C(V_G)\right]d(\omega t)\right\} \tag{26}$$

and

$$V_N \equiv \frac{\ell}{2L} R_L V_0^2 \omega\left\{\frac{1}{V_0}\frac{4}{\pi}\int_0^{\pi/2}\left[C(v_{G+}) - C(v_{G-})\right]\sin 2\omega t \sin\omega t \, d(\omega t)\right\} \tag{27}$$

The approximate solution, eqs. (25)-(27), is expected to closely approach the exact solution in the majority of envisioned applications, and, of course, reduces to the eq. (21) solution in the small signal limit. Capacitance-voltage relationships which were used in conjunction with eqs. (25)-(27) to obtain the Fig. 5(a) results are included in Appendix 2.

Of note in examining Fig. 5(a) is the excellent agreement (to better than 1%) between the exact and approximate solution results, thereby validating use of the approximate solution. One also notes the qualitatively predicted (and experimentally observed[8,9,13,14]) bell-shaped form of the characteristics. With increasing signal level the peak of these characteristics diminishes in magnitude and shifts toward inversion, while the output in general is seen to be significant over a larger

voltage range. Finally, it should be pointed out that the large signal characteristics have been extended a distance $2V_0$ past the start of inversion using a formalism strictly valid only for accumulation and depletion biases. The reason for this extension will become obvious after we have discussed the inversion bias response.

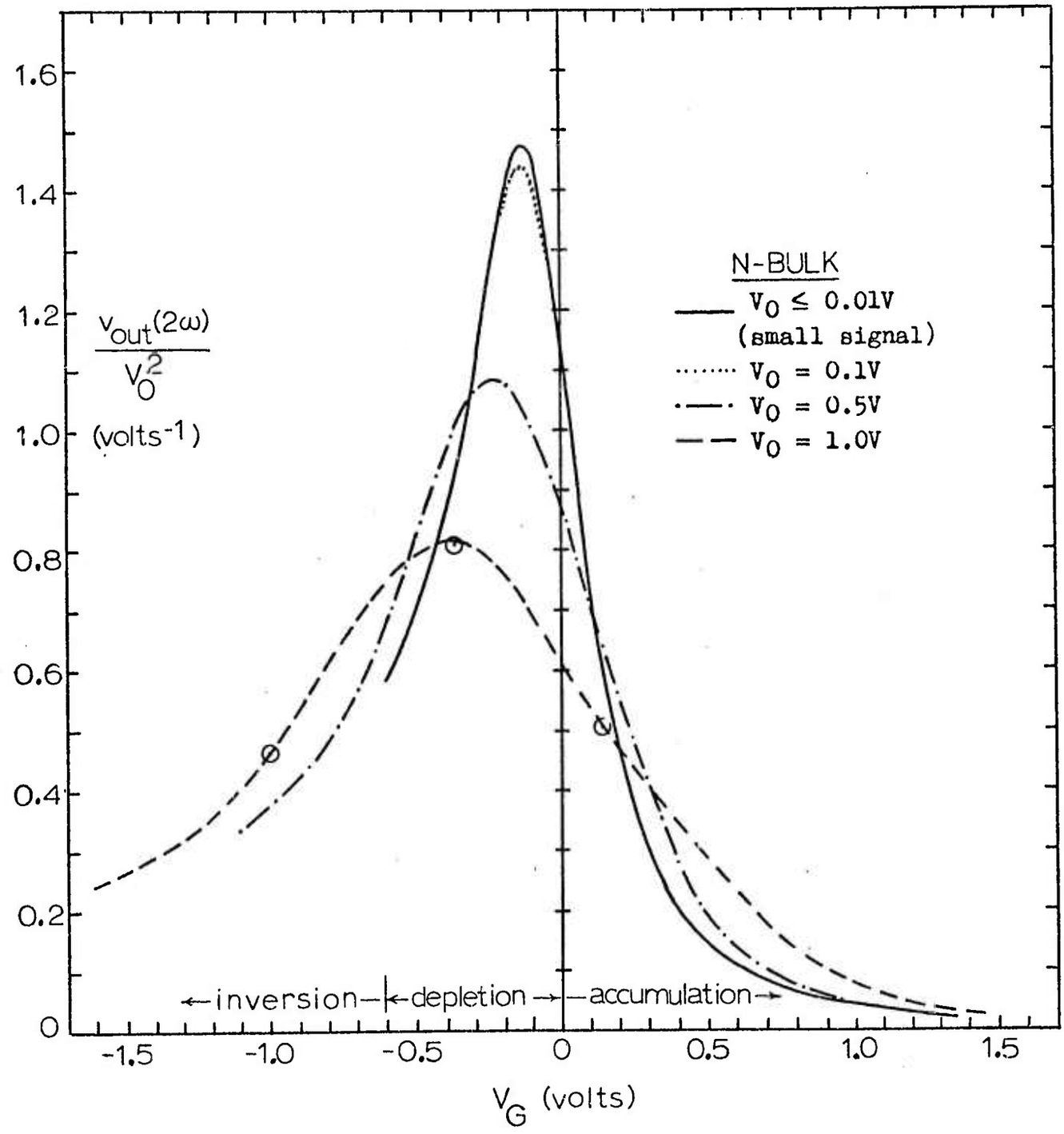

FIG. III-5A

Sample computational results illustrating the effect of signal level on the convolver output characteristics.

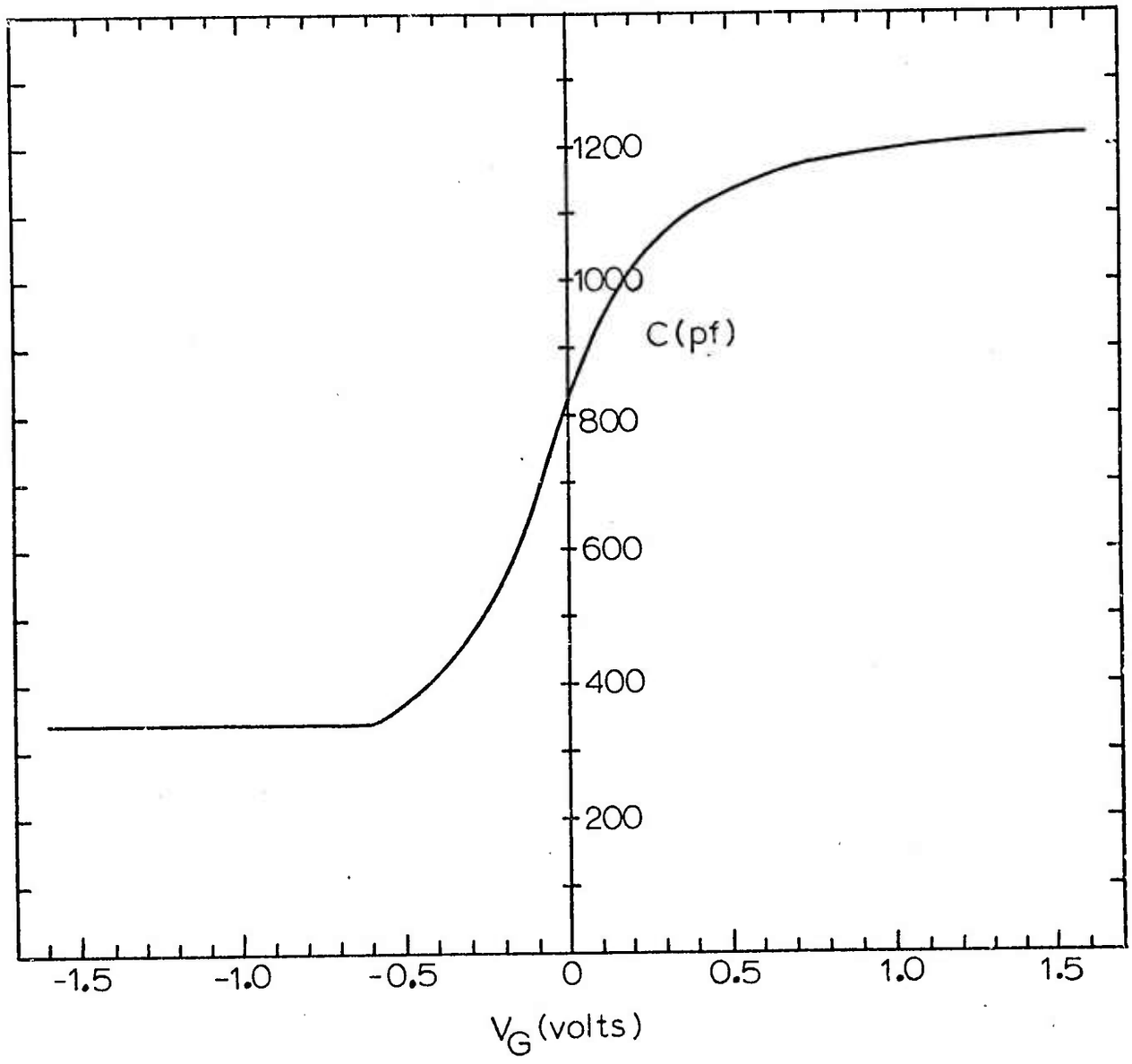

FIG. III-5B

Corresponding high frequency capacitance vs. voltage characteristics. 0 denotes exact solution results. A complete list of measurement and ZnO-SiO_2-Si structural parameters assumed in performing the computations is tabulated in Appendix 1.

6. INVERSION BIAS RESPONSE

For accumulation and depletion biasing of the ASW convolver the response analysis is relatively straightforward because only majority carriers are involved in the operation of the device. Under inversion biasing, however, the situation changes drastically; minority carrier generation, minority carrier recombination, and the lateral transfer of minority carriers between adjacent half-wavelengths in the overlap region must all be considered in establishing the structure's response.

Let us first examine the expected inversion bias response assuming minority carriers cannot transfer between adjacent half-wavelength regions; i.e., assuming the Fig. 3a MIS capacitors are simple isolated circuit components. At the high frequencies encountered in the ASW convolver and provided the signal magnitude is relatively small, very little minority carrier generation-recombination will take place in any given cycle and the capacitance vs. voltage locus followed by an isolated MIS-C will be that of curve (a) sketched in Fig. 6a. This capacitance vs. voltage dependence will be essentially independent of inversion bias and will be functionally equal to the deep depletion capacitance-voltage dependence observed at the inversion-depletion transition point (V_T in Fig. 6a). Hence, $v_{out}(2\omega)$ in the small-signed no-interaction limit is predicted to be a well defined bias independent constant under inversion biasing.

For larger signal levels in the no-interaction limit minority carrier generation still proceeds at a negligible rate. However, carrier recombination increases at a rapid rate with excursions above the high-frequency capacitance and initially leads to the capacitance-voltage locus of curve (b) in Fig. 6a at sufficiently high signal levels. (The situation

is similar to that in a forward biased pn junction.) The removal of minority carriers from the system during the first few cycles in turn causes the capacitance vs. voltage locus to quickly settle along the Fig. 6a curve (c) locus where again both generation and recombination proceed at a negligible rate per cycle. This capacitance vs. voltage dependence will be essentially independent of inversion bias and will be functionally equal to the deep depletion capacitance-voltage dependence observed at a bias $|V_G| > |V_T|$. Hence, the inversion bias large-signal no-interaction $v_{out}(2\omega)$ is predicted to be a bias independent constant and, as can be readily established, will be somewhat smaller than the small signal $v_{out}(2\omega)$, (see Fig. 6b).

The preceding analysis suffers from the fact that the lateral transfer of minority carriers between adjacent half-wavelength regions cannot be ignored. Actually, the inversion bias situation inside the ASW convolver is very similar to a charge coupled device (CCD) if one were to apply equal and opposite clock pulses to alternate CCD gates (corresponding to alternate half-wavelength regions). As one set of gates (half-wavelength regions) is driven further into inversion thereby calling for an increase in minority carrier charge, the second set of gates (half-wavelength regions) is driven back toward depletion tending to build up an excess of minority carrier charge. In both structures the proximity of adjacent regions and existing lateral fields clearly favor a lateral transfer of minority carriers as illustrated in Fig. 7a.

If the charge transfer were totally efficient, then changes in the minority carrier charge would track and cancel changes in the effective surface wave charge (Q'_{ss}), leading to an identically zero convolver output

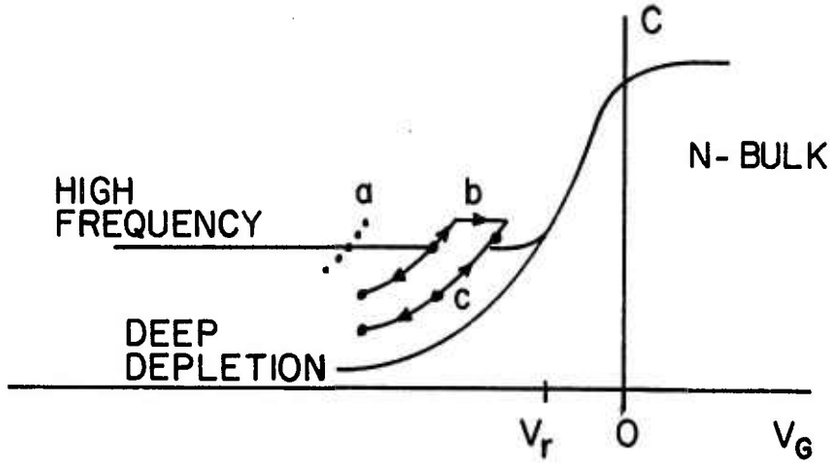

FIG. III-6a

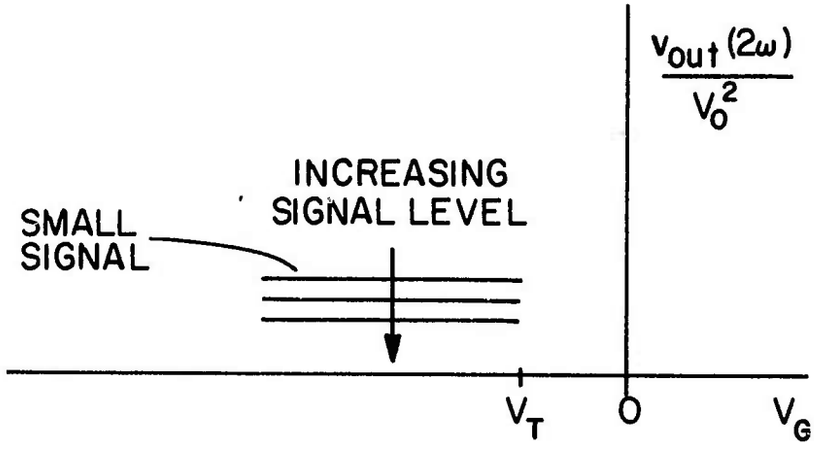

FIG. III-6b

(a) The small signal capacitance vs. voltage dependence exhibited by an MIS-capacitor when the gate bias is rapidly modulated about an inversion bias point will typically follow curve (i) at relatively small signal levels and curve (ii) (initially) and curve (iii) (after repeated excursions) at large signal levels. (b) Expected inversion bias convolver output if one ignores the lateral transfer of minority carriers between adjacent half-wavelength regions.

once the voltage swing on half-wavelength regions was totally contained in the inversion bias range. However, from the analysis of surface channel CCD's one finds a relatively poor transfer inefficiency at low minority carrier concentrations (especially at typical ASW convolver frequencies). The transfer efficiency improves rapidly with increasing minority carrier concentration and the overall transfer efficiency should also depend on the total number of carriers to be transferred. Using this information we conclude the no-interaction analysis will be approximately valid near the start of inversion, but lateral charge transfer will gradually decrease the response as one progresses into the inversion bias range yielding the envisioned response of Fig. 7b.

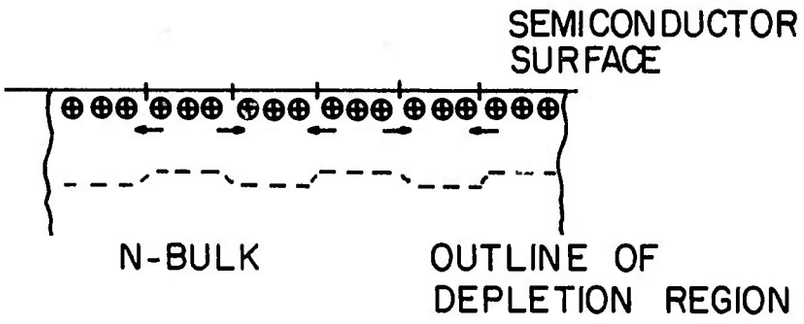

FIG. III - 7a

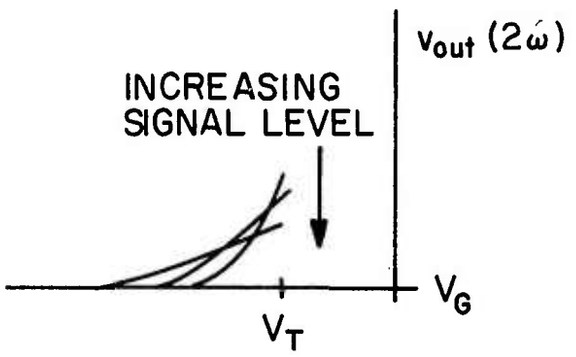

FIG. III - 7b

(a) Visualization of lateral minority carrier motion in an inversion biased convolver. (b) Expected inversion bias convolver output taking into account the lateral transfer of minority carriers between adjacent half-wavelength regions.

IV. Acoustic Surface Wave Measurement of Majority Carrier Mobility*

(R. F. Pierret and R. L. Gunshor)

In a recent publication Bers, et al.[1] utilized acoustic surface wave (ASW) techniques to ascertain the effective mobility of near surface carriers in a semiconductor accumulation layer. Their experimental configuration consists of a high resistivity n-silicon sample placed on top of a lithium niobate substrate. The ASW is launched on the lithium niobate, and propagates under the silicon. The piezoelectric fields associated with the ASW tend to produce a drift of electrons along the direction of propagation. The resulting direct current, called an acoustoelectric current, is measured and used to compute the value of the surface mobility. The cited paper was significant in that it illustrated the potential of ASW techniques in probing semiconductor surface properties.

We note that the appropriate theory for majority carriers in accumulations layers was first formulated by Greene, et al.[2] and was later presented in a more convenient form by Goldstein, et al.[3] For the Bers, et al. structures and the normalized surface potential (U_S) range probed, the theoretical effective mobility to bulk mobility ratio (μ_{eff}/μ_B) is accurately approximated by

$$\frac{\mu_{eff}}{\mu_B} = 1 - \frac{r}{\sqrt{2}} e^{-U_S/2} \int_{U_S-7}^{U_S} e^{x}[1 - e^{-f(x)/r}]dx \qquad (1)$$

where

$$f(x) = e^{-x/2} \operatorname{erf}\sqrt{(U_S-x)/2} \qquad (2)$$

*To appear in the Journal of Applied Physics.

and r = 0.001. The preceding majority carrier theory and the Bers, et al. experimental results are compared in Fig. IV-1. Very good agreement between the corrected theoretical predictions and the ASW measured mobilities is clearly evident.

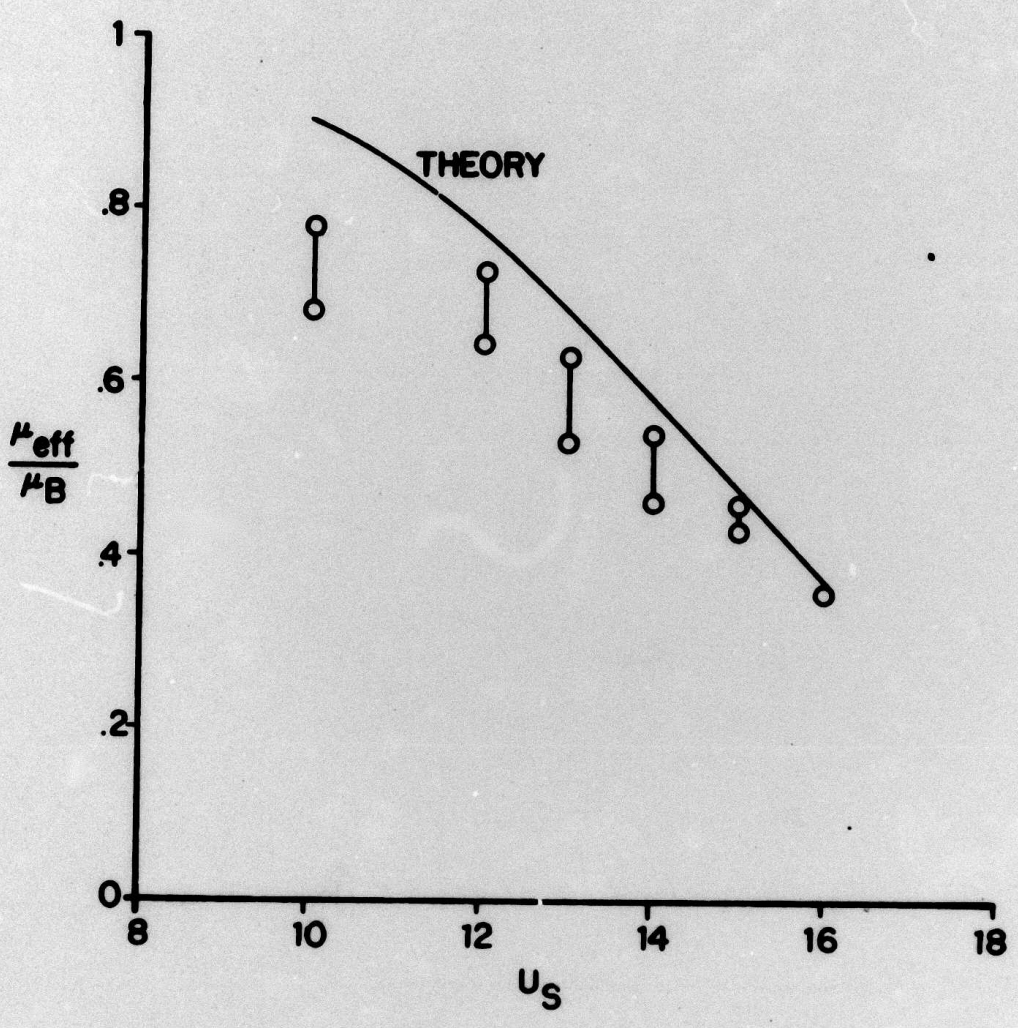

FIG. VI-1 Comparison of accumulation layer effective mobility theory and ASW derived experimental results. (O—O range of Bers et. al data derived from three similar test structures.)

References

1. A. Bers, J. H. Cafarella and B. F. Burke, "Surface Mobility Measurements Using Acoustic Surface Waves," Appl. Phys. Letts., 22, 399 (April 15, 1973).

2. R. F. Greene, D. R. Frankl and J. Zemel, "Surface Transport in Semiconductors," Phys. Rev., 118, 967 (May, 1960).

3. Y. Goldstein, N. B. Grover, A. Many, and R. F. Greene, "Improved Representation of Calculated Surface Mobilities in Semiconductors. II. Majority Carriers," J. A. P., 32, 2540 (December, 1961).